ACCELERATION IN VERTICAL ORBIT EXCURSION FFAGs WITH EDGE FOCUSSING

S.J. Brooks*, RAL, Chilton, OX11 0QX, UK

Abstract

FFAGs with vertical orbit excursion (VFFAGs) provide a promising alternative design for rings with fixed-field superconducting magnets. They have a vertical magnetic field component that increases with height in the vertical aperture, yielding a skew quadrupole focussing structure. Edge focussing can provide an alternating gradient within each magnet, thus reducing the ring circumference. Like spiral scaling horizontal FFAGs (but not non-scaling ones) the machine has fixed tunes and no intrinsic limitation on momentum range. Rings to accelerate the 800 MeV beam from the ISIS proton synchrotron are investigated, in terms of both magnet field geometry and longitudinal behaviour during acceleration with space charge. The 12 GeV ring produces an output power of at least 2.18 MW.

MAGNET FIELD MODEL

The field within the body of a VFFAG magnet is given by $B_y = B_0 \mathrm{e}^{ky}$ on the $x = 0$ mid-plane. The beam travels in the $+z$ direction through the magnet and shifts to height $y = \frac{1}{k} \ln p/p_{\mathrm{inj}}$ as momentum p increases, so the injection orbit is at $y = 0$ and the current windings lie on the $\pm x$ sides of the vertical gap. Optics of a ring with such magnets without edge effects are considered in [1]. At injection, the magnet body has bending field B_0 and skew gradient $B_0 k$ (as well as higher multipoles of strength proportional to $B_0 k^{n\geq 2}$), so without edge effects B_0 must alternate in sign to provide alternating gradient focussing. k must be constant for the entire ring to satisfy the scaling law

$$y \mapsto y + \Delta y, \qquad (p, \mathbf{B}) \mapsto (p, \mathbf{B})\mathrm{e}^{k\Delta y},$$

which ensures the orbit shape and tunes are preserved during acceleration. Having negative B_0 for some magnets produces reverse bends and increases machine circumference for a given field by $\sim$5 times, similar to the circumference factor [2] in horizontal scaling FFAGs.

To represent magnets with edges, the parameter $\tau = \tan\theta_{\mathrm{edge}}$ is introduced, along with a coordinate $\zeta = z - \tau y$ so that the magnet corresponds to the region $0 \leq \zeta \leq L_{\mathrm{mag}}$ for all y. Field fall-off is determined by a function $f(\zeta)$ that approaches 1 in the magnet body and 0 outside. Naively one wants a mid-plane field $B_y = B_0 \mathrm{e}^{ky} f(\zeta)$ but to obey Maxwell's equation $(\nabla \times \mathbf{B})_x = 0$, this has to be modified to $(B_y, B_z) = B_0 \mathrm{e}^{ky} \left(f(\zeta) - \frac{\tau}{k} f'(\zeta), \frac{1}{k} f'(\zeta) \right)$. The note [3] derives this formula and the Taylor series extrapolation used to calculate fields for $x \neq 0$. For edge angles, $z \mapsto z + \tau \Delta y$ is added to the VFFAG scaling law to keep ζ constant (more accurately, this is a rotation of $\tau \Delta y / R$ about the ring centre).

* stephen.brooks@stfc.ac.uk

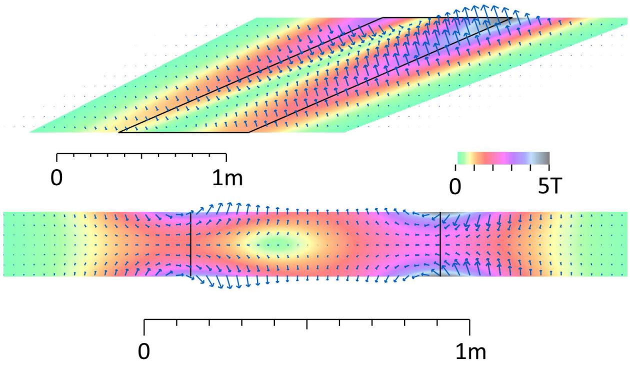

Figure 1: Cross-section of the 5 GeV ring magnet's field in ZY (top) and ZX (bottom) planes.

The resulting field is plotted in figure 1. The fringe field at the entrance to the magnet has opposite sign to that at the exit, providing alternating gradient focussing without changing the sign of B_0. Note that symmetry about the YZ plane forbids conventional quadrupole fields, meaning all focussing is skew apart from the solenoidal component B_z.

Field Enhancement Factor

As can be seen in figure 1, the largest fields are present in the magnet edges and off-plane. The field enhancement factor $\max_z |\mathbf{B}(x, y, z)|/(B_0 \mathrm{e}^{ky})$ is plotted in figure 2 (at $y = 0$, though by the scaling law it is the same at all y).

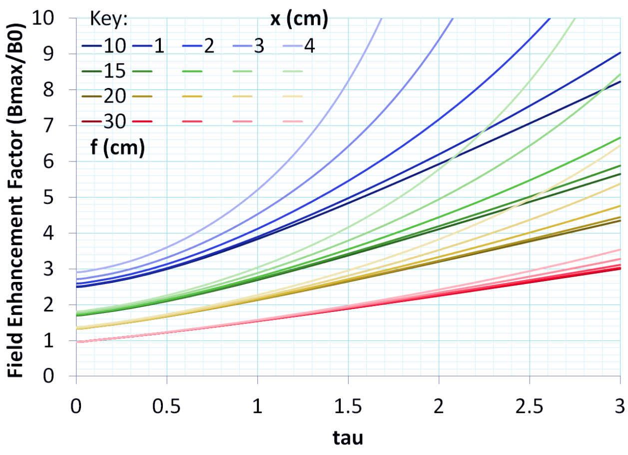

Figure 2: Field enhancements as a function of τ, fringe length (f) and distance from mid-plane (x) from 0 to 4 cm, in the 3 or 5 GeV magnet design with $k = 2.05\,\mathrm{m}^{-1}$.

Enhancement increases with τ but is ameliorated by increasing fringe length; it also increases extremely rapidly with x for small fringe lengths. However, it decreases with increasing k because higher k magnets actually have weaker fringe fields.

In ring design, this number fills a similar role to the circumference factor of scaling FFAGs: it is the amount a theoretical plain bending field must be multiplied by to find the real maximum field strength in a ring of fixed size and magnet filling factor.

TRANSVERSE DYNAMICS

Parameters were sought for fixed-field rings to boost the energy of the two ISIS [4] proton bunches from 800 MeV, following the outline RF approach in [5]. Lattice cells containing a single VFFAG magnet and a reasonably-long drift space, with enough dynamic aperture for the 150 mm.mrad geometric emittance proton beam are given in table 1.

Table 1: Transverse Parameters for VFFAG Rings

$E_{k,\text{inj}}$	800 MeV		
$E_{k,\text{ext}}$	3 GeV	5 GeV	12 GeV
Mean radius	52 m (2×ISIS)		
Superperiods	80 (superperiod is one cell)		
Cell length	4.0841 m		
Drift length	3.3174 m		3.1257 m
Magnet Parameters			
Magnet length	0.7667 m		0.9584 m
B_0	0.5 T		0.4 T
k	2.05 m^{-1}		2.23 m^{-1}
$\tau = \tan\theta_{\text{edge}}$	2.3		2.6
θ_{edge}	66.50°		68.96°
Fringe length	$f = 0.3$ m in $B \propto \frac{1}{2} + \frac{1}{2}\tanh(z/f)$		
B_{ext}	1.3069 T	2.0036 T	3.5274 T
$B_{\text{fringe}}/B_{\text{body}}$	$2.7251_{x=4\,\text{cm}}$		$2.6399_{x=2\,\text{cm}}$
$B_{\max}$	3.5615 T	5.4600 T	9.3119 T
Beam Optics			
$y_{\text{ext}} - y_{\text{inj}}$	0.4687 m	0.6771 m	0.9762 m
μ_u (per cell)	71.11°		71.33°
μ_v	28.68°		19.65°
Q_u (ring)	15.802		15.851
Q_v	6.373		4.367

The beam power will increase in proportion to energy, so options are provided for neutron production at 3 GeV, high-power exotics production at 12 GeV and a 'compromise' energy of 5 GeV, which provides more power for neutrons but perhaps less efficiency. With the mean current 208 μA presently achievable in ISIS, these would have beam powers of 0.6, 2.5 and 1.0 MW respectively at 50 Hz.

The 12 GeV ring, the most aggressive design, with applications to neutrino factories and muon colliders, needed a slightly longer magnet to lower the peak field, which in turn required larger edge angles. The field enhancement was evaluated at $x = 2$ cm and not 4 cm to account for adiabatic shrinkage of the beam once accelerated to 12 GeV.

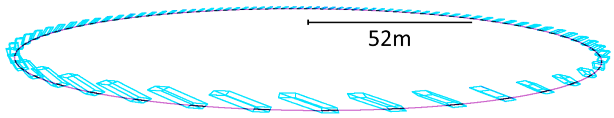

Figure 3: Perspective view of the 12 GeV ring.

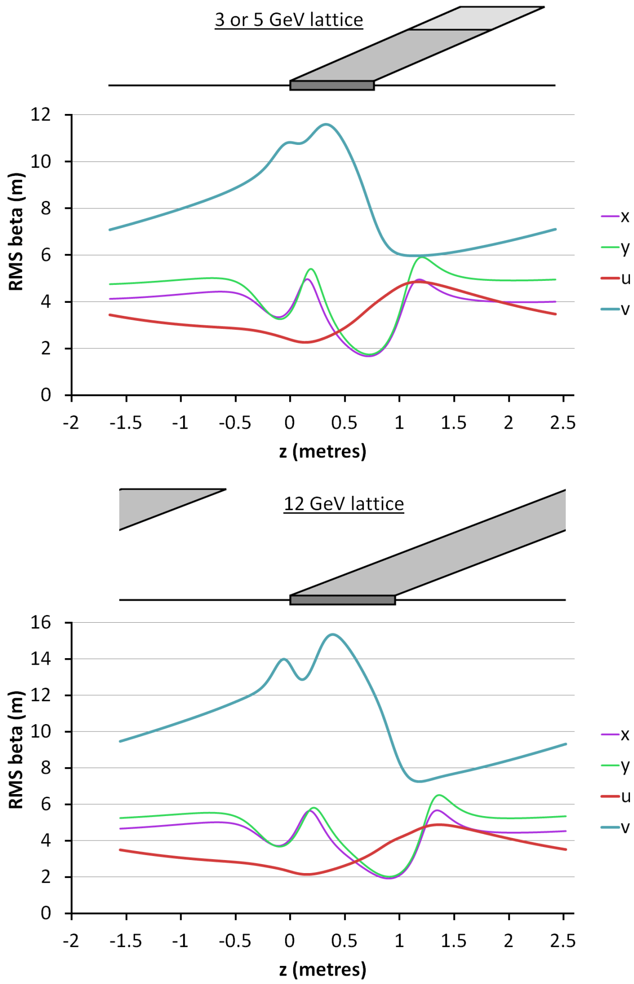

Figure 4: Beta functions in the two lattices, in non-skew and skew coordinates. Magnet size is to scale in z and y.

In terms of skew coordinates

$$u = (x + y)/\sqrt{2} \qquad \text{and} \qquad v = (y - x)/\sqrt{2},$$

the lattice beta functions shown in figure 4 are overall doublet-like but with some features in the end fields. The cell and machine tunes in table 1 are also given in terms of u and v. The x and y optics are highly coupled so do not behave like normal beta functions. Figure 5 shows how the phase spaces vary through the magnet, with some distortion of the matched shape, particularly in the (v, v') plane due to nonlinearity in the magnetic field.

The scaling law gives VFFAGs interesting properties, such as constant dispersions $D_x = 0$ and $D_y = \frac{1}{k}$ and a constant orbit length that makes $\gamma_{tr} = \infty$.

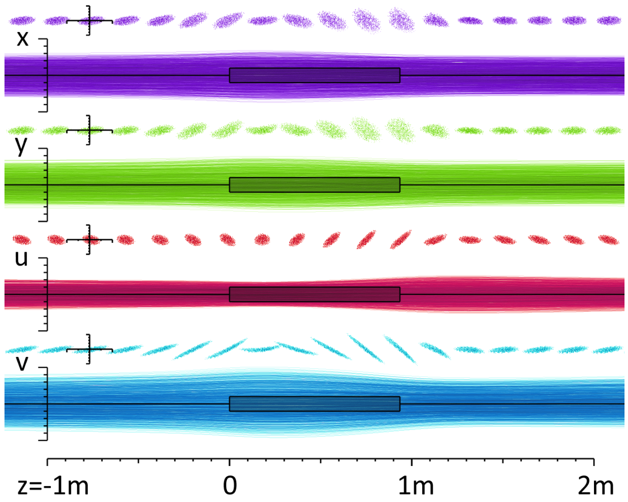

Figure 5: Phase space and beam evolution through the 12 GeV ring cell at injection energy. Transverse scale is ±5 cm and x', y', u', v' ranges are ±20 mrad.

Dynamic Aperture Parameter Scan

The ring designs were found as combinations of six parameters $(B_0, k, \tau, f, L_{\mathrm{mag}}, L_{\mathrm{drift}})$, the last two being dictated by the integer RF harmonic number (ring circumference) and superperiodicity (cell length) together with B_0, which gives the magnet fill factor. The main focussing parameters k and τ were scanned over, producing plots like figure 6. For each square, 250 protons from a 150 mm.mrad waterbag beam were tracked for 250 cells and removed if $r > 10$ cm. Squares are coloured according to the percentage that survive, showing areas of good dynamic aperture.

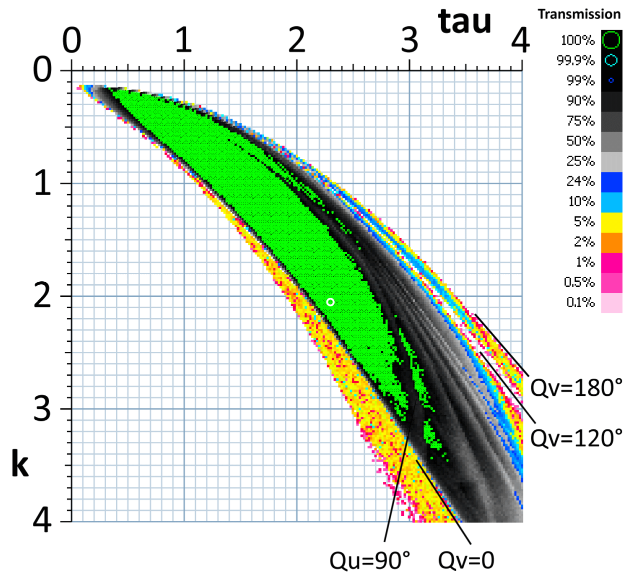

Figure 6: Proton beam transmission as a function of τ and k, with the 3 or 5 GeV ring design circled. Lines of increased loss correspond to cell tune resonances (labelled).

Transverse Intensity Issues

Since the ring tune is 80 times the cell tune, a fine-tuning stage is needed to steer the fractional parts of the ring tunes away from resonances. For the 3 or 5 GeV ring,

$$\frac{\partial Q_{u,v}}{\partial k} = \begin{bmatrix} -8.49 \\ -94.46 \end{bmatrix} \quad \text{and} \quad \frac{\partial Q_{u,v}}{\partial \tau} = \begin{bmatrix} 39.92 \\ 119.82 \end{bmatrix},$$

which are linearly independent enough to find any desired fractional ring tunes without major deterioration of the optics. This fine-tuning will also have to be done on the real machine, using trim coils producing fields proportional to $\partial\mathbf{B}/\partial k$ and $\partial\mathbf{B}/\partial\tau$.

The rapid variation of Q_v arises because the cell tune in v is quite close to zero. This is problematic since Q_v also varies rapidly in response to space charge forces, making the tune depressions of these rings roughly $\Delta Q_{sc,u} = -0.2$ and $\Delta Q_{sc,v} = -0.4$ at injection. This could be improved by finding rings with more balanced tunes or larger mean beta functions, though maybe at the expense of shorter drift spaces or a larger circumference.

LONGITUDINAL DYNAMICS

The line charge density ρ_{1D} along the beam determines the level of transverse as well as longitudinal space charge, so it is important to do realistic simulations of the longitudinal bunch shape including space charge. The simulation code written for this uses three transformations on the particle $(\Delta t, \Delta E)$ coordinates: a drift, an RF kick and a space charge kick; doing these once per turn provides sufficient accuracy. The drift affects Δt depending on the ring circumference function $C(E_k, t)$. For a synchrotron, the absolute time t determines the machine magnet reference momentum p_0, then the particle's E_k gives its $\Delta p/p$, so to first order $C = C_0(1 + \alpha_0 \Delta p/p)$ where α_0 is the momentum compaction (0.0392 for ISIS). Fixed field magnets have no t dependence and for a VFFAG the circumference does not change with closed orbit momentum either, so C is constant. The RF and space charge kicks affect ΔE only, so when done separately from the drift, phase space area is preserved.

RF voltages applied to a proton per turn are defined as $-V_0 \sin(\phi_0 + 2\pi f \Delta t)$, with $V_0(t), \phi_0(t)$ specified by the user. Space charge is calculated using the derivative of the line density, which is Gaussian-smoothed to reduce statistical noise. Provided $\frac{\mathrm{d}^2\rho_{\mathrm{1D}}}{\mathrm{d}z^2}$ is small, the voltage per turn from space charge is

$$V_{\mathrm{sc}} = -C\,\langle E_{z,\mathrm{sc}}\rangle = \frac{C}{4\pi\epsilon_0}\frac{g}{\gamma^2}\frac{\mathrm{d}\rho_{\mathrm{1D}}}{\mathrm{d}z},$$

where g is a shielding factor from the shape of the beam and the conducting beam pipe [6]. ISIS has $g = 1.546$ in a mostly round beam pipe, while the VFFAG has $g = 1.914$ for a skew Gaussian beam between two vertical conducting plates at $x = \pm 4$ cm, calculated using the method in [7].

To obtain an input distribution for the VFFAG (and as a check), 1D simulations were first run on ISIS starting from

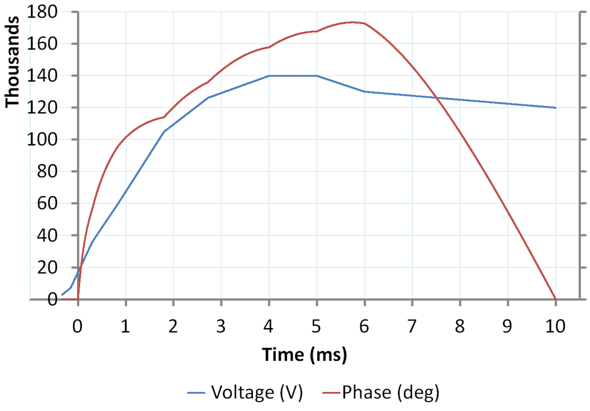

Figure 7: ISIS first harmonic RF program.

the linac injection at 70.44 MeV. The voltage and phase functions [8] for this are shown in figure 7 and the results in figure 8 agree with the current models and observed transmission values of the machine in this mode.

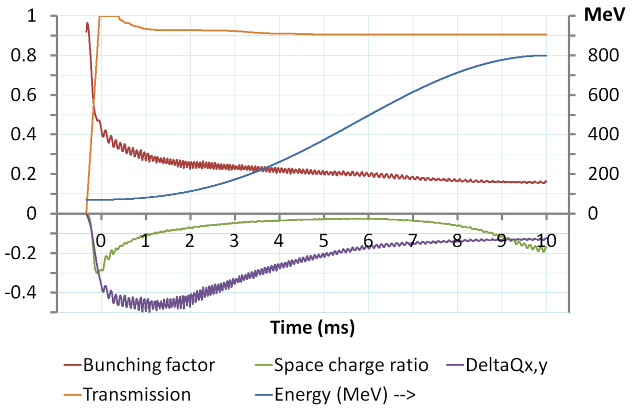

Figure 8: Bunching factor, transmission and intensity-dependent effects in the ISIS first harmonic simulation.

Longitudinal Intensity Effects

Figure 8 shows a number of parameters that could limit machine intensity. The bunching factor is defined as $B = \langle\rho_{1D}\rangle / \rho_{1D}^{\mathrm{peak}}$ with smaller values being worse for space charge. The 'space charge ratio' is defined as an average of $V_{\mathrm{sc}}/V_{\mathrm{rf}}$ over the beam, roughly equivalent to $\Delta Q_s/Q_s$ in terms of the synchrotron tune. It has been shown using the Boussard criterion [9] that this must be greater than -0.4 to avoid microwave instabilities. To avoid dividing by zero when $V_{\mathrm{rf}} = 0$, the ratio is actually calculated as the weighted average $\sum V_{\mathrm{sc}} V_{\mathrm{rf}} / \sum V_{\mathrm{rf}}^2$.

Transverse tune shifts are calculated using the Laslett tune shift formula without boundary terms:

$$\Delta Q_{x,y} = -\frac{q^2}{4\pi\epsilon_0 mc^2} \frac{N}{2\pi B\beta\gamma^2\epsilon_{x,y}^{\mathrm{n,rms}}} \frac{\bar{\sigma}_{x,y}}{\bar{\sigma}_x + \bar{\sigma}_y},$$

where the last term only requires the average beam aspect ratio $\bar{\sigma}_x/\bar{\sigma}_y$, which is 1 for ISIS and $\bar{\sigma}_u/\bar{\sigma}_v = 0.554$ for the 12 GeV VFFAG. There is a slight inconsistency with the transverse simulations that used a waterbag with $\epsilon_{x,y}^{\mathrm{rms,800MeV}} = 25$ mm.mrad whereas the 1D simulations assumed the value 30 mm.mrad observed in the machine.

VFFAG RF System

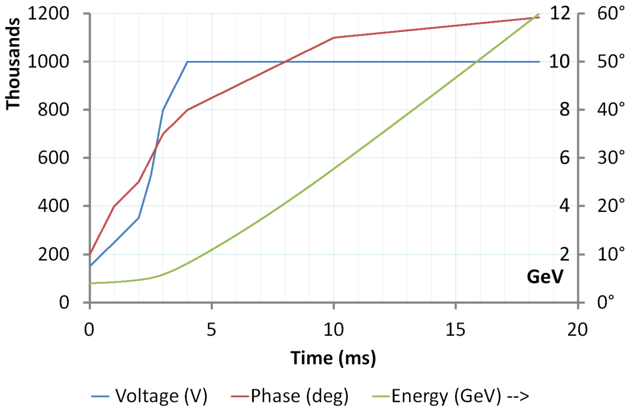

Figure 9: RF acceleration program for the 12 GeV VFFAG.

The VFFAG transfers the two bunches from ISIS into the 1$^{\mathrm{st}}$ and 3$^{\mathrm{rd}}$ buckets of a frequency-doubled RF system given in table 2. Because of this doubling, the bunch initially fills much of the RF bucket, meaning only low acceleration phases are possible early in the cycle (figure 9). Later on, the bunch shrinks in time spread and increases in energy spread (figures 11,12), allowing faster acceleration.

Table 2: Longitudinal parameters for the 12 GeV VFFAG. Peak voltage per turn and phase are linearly interpolated from the times given.

RF harmonic	$h = 8$	
RF frequency	6.179–7.321 MHz	
Cycle duration	18.41 ms	
Rep. rate	50 Hz	
Time (ms)	**Voltage (kV)**	**Phase**
0	150	10°
1	250	20°
2	350	25°
2.5	525	30°
3	800	35°
4	1000	40°
10	1000	55°
18.41 (extract)	*1000*	*59.21°*
20	1000	60°

In theory the bunch could be adiabatically compressed via an increase in RF voltage early in the cycle, followed by high-phase acceleration. However, as figure 10 shows, at low energies of 0.8–1.1 GeV (the first 3 ms) the tune shift in the v plane is high and would exceed the half integer limit if full bunch compression was attempted near injection energy, hence the period of low-phase acceleration.

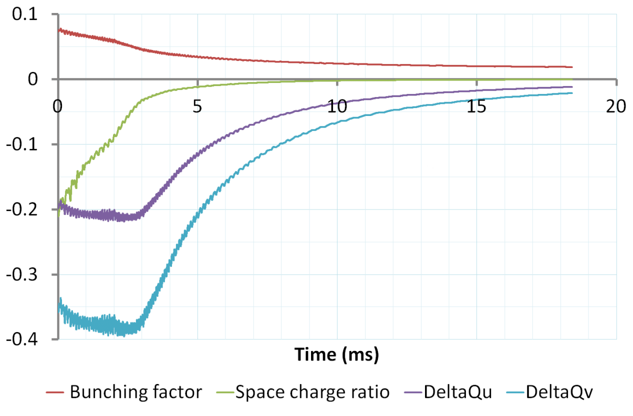

Figure 10: Bunching factor and intensity-dependent effects in the 12 GeV VFFAG simulation.

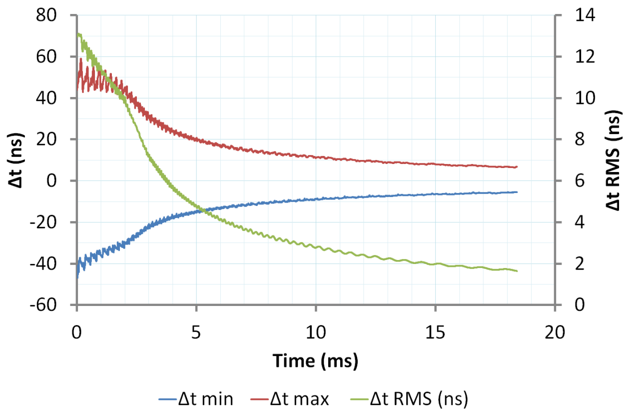

Figure 11: Bunch duration in the 12 GeV VFFAG simulation, reducing to a final value of $\Delta t_{\mathrm{rms}} = 1.64$ ns.

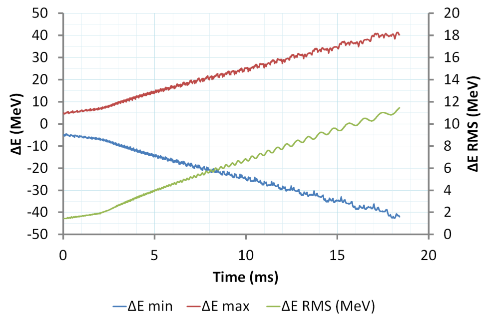

Figure 12: Increase of bunch energy spread in the 12 GeV VFFAG simulation to ± 41.1 MeV.

Table 3: Intensity-dependent parameters for the ISIS single harmonic and 12 GeV VFFAG simulations run in series, for different numbers of protons injected into ISIS.

ISIS Protons In	**2.50e13**	**2.75e13**	**3.00e13**
ISIS μA in	200.3	220.3	240.3
ISIS transmission	90.54%	87.95%	85.98%
ISIS protons out	2.26e13	2.42e13	2.58e13
ISIS μA out	181.3	193.7	206.6
ISIS power (kW)	145	155	165
VFFAG transmission		100%	
VFFAG power (MW)	2.18	2.32	2.48
ISIS Peak Intensities			
Bunching factor	0.154	0.150	0.151
Space charge ratio	-0.301	-0.305	-0.311
$\Delta Q_{x,y}$	-0.499	-0.544	-0.580
VFFAG Peak Intensities			
Bunching factor	0.0188	0.0190	0.0190
Space charge ratio	-0.211	-0.257	-0.278
ΔQ_u	-0.219	-0.240	-0.254
ΔQ_v	-0.395	-0.434	-0.458

Table 3 shows the result of increasing the ISIS linac pulse length by 10 or 20%. Worst-case intensity parameters are shown, which are reasonable for the VFFAG even with 14% more current, although in reality ISIS would use a more efficient RF program or its 2^{nd} harmonic system.

Although there is enough horizontal drift space for the proposed RF at 25% packing factor [5], the diagonal shape of the gap may be problematic. Later designs may use a racetrack VFFAG with large edge angles only in the bends.

Suitability for Muon Production

Note that in figure 11, the output RMS bunch length is small enough to be used for a neutrino factory proton driver [10]. Some of the 1.59 ms spare time for RF reset at the end of the cycle could be used to produce an energy flat top so the two bunches can be extracted with a delay between.

REFERENCES

[1] *Vertical Orbit Excursion FFAGs*, S.J. Brooks, Proc. HB2010.

[2] *The FFAG Synchrotron—Mark I*, K.R. Symon, MURA note 043 (1954).

[3] *Fringe Fields for VFFAG Magnets with Edge Angles*, S.J. Brooks, available from `http://stephenbrooks.org/-ral/report/2011-6/skewVFFAGfringes.pdf` (2011).

[4] *Spallation Neutron Source: Description of Accelerator and Target*, ed. B. Boardman, Rutherford Appleton Laboratory technical report RL-82-006 (1982).

[5] *Extending the Energy Range of 50 Hz Proton FFAGs*, section 'Design Parameters', S.J. Brooks, Proc. PAC 2009.

[6] *Form Factor g In Longitudinal Space Charge Impedance*, R. Baartman, TRIUMF design note 1992-TRI-DN-K206, available from `http://lin12.triumf.ca/text/-design_notes/k206/k206h.pdf`.

[7] *Arbitrary Beams in Uniform Pipes*, S.J. Brooks, section 2.6.2 'Elliptical Gaussian Beam', available from `http://stephenbrooks.org/ral/report/2012-6/-abeamupipe.pdf` (2012).

[8] C.R. Prior (RAL), private communication.

[9] *Bunches with Local Elliptic Energy Distribution*, A. Hofmann and F. Pedersen, section 'Microwave instabilities', Proc. PAC'79.

[10] *Interim Design Report*, The IDS-NF collaboration, table V 'Proton driver requirements', p.55, RAL-TR-2011-018.